Closed-Loop Recyclable High-Performance Polyimine Aerogels Derived from Bio-Based Resources

ADVANCED MATERIALS
www.advmat.de

Closed-Loop Recyclable High-Performance Polyimine Aerogels Derived from Bio-Based Resources

*Changlin Wang, Fabian Eisenreich, and Željko Tomović**

Organic aerogels are an intriguing class of highly porous and ultralight materials which have found widespread applications in thermal insulation, energy storage, and chemical absorption. These fully cross-linked polymeric networks, however, pose environmental concerns as they are typically made from fossil-based feedstock and the recycling back to their original monomers is virtually impossible. In addition, organic aerogels suffer from low thermal stability and potential fire hazard. To overcome these obstacles and create next-generation organic aerogels, a set of polyimine aerogels containing reversible chemical bonds which can selectively be cleaved on demand is prepared. As precursors, different primary amines and cyclophosphazene derivatives made from bio-based reagents (vanillin and 4-hydroxybenzaldehyde) to elevate the thermal stability and reduce the environmental impact are used. The resulting polyimine aerogels exhibit low shrinkage, high porosity, large surface area, as well as pronounced thermal stability and flame resistance. More importantly, the aerogels show excellent recyclability under acidic conditions with high monomer recovery yields and purities. This approach allows for preparation of fresh aerogels from the retrieved building blocks, thus demonstrating efficient closed-loop recycling. These high-performance, recyclable, and bio-based polyimine aerogels pave the way for advanced and sustainable superinsulating materials.

1. Introduction

Reducing the dependence of our society on energy-demanding activities has gained extensive attention since we are facing an unprecedented growth of worldwide energy consumption, rising energy costs, and associated environmental issues. In particular, the thermal insulation of buildings is critical since it accounts for ≈40% of the global energy demand.[1,2] To tackle this problem, insulating materials with the lowest possible thermal conductivity are used to reduce the heat loss of buildings to the external environment. Among the insulating materials, aerogels show minimal thermal conductivities below 0.020 W m^{-1} K^{-1},[3–6] which are superior to other commercial insulators (e.g., mineral wools, polymer foams).[7] Aerogels are porous materials containing confined air molecules that feature small pore size, extremely low density, high porosity, and high specific surface area.[3,4] The isotropic nanostructure of aerogel restricts the mobility of occupied gas molecules and thus inhibits collision of gas molecules (known as Knudsen effect).[8,9] Consequently, the thermal conductivity of aerogels through convective heat flow is strongly reduced, which is the foundation for their superinsulating performance.

Organic aerogels comprise a versatile range of cross-linked synthetic polymeric materials, such as resorcinol-formaldehyde,[10] polyurethanes,[11–13] polyureas,[14,15] and polyimides.[16–19] Their preparation is typically achieved by sol–gel synthesis and subsequent supercritical drying to remove the solvent without disrupting the polymer skeleton. Because the polymeric networks are constructed with covalent C—C bonds, organic aerogels endow greater mechanical properties than commercial silica aerogels.[20,21] In addition, organic aerogels provide ample design space for creating advanced materials by tailoring their framework via chemical transformations and derivatization. However, well-established organic aerogels, such as resorcinol-formaldehyde aerogels[4,10] and polyurea aerogels,[14,15] show relatively low thermal stability. To improve the heat resistance and diminish fire hazards, precursors or additives with high thermal stability have been incorporated into the aerogel architecture (e.g., melamine,[22,23] polybenzoxazole,[24–26] isocyanurate,[27] imide,[16,19] and phosphazenes[28]).

Besides the potential flame risk, other concerns of organic aerogel are their sustainability and end-of-life management. The aerogel production requires large quantities of fossil-based feedstocks, such as resorcinol, formaldehyde, and isocyanates. Hence, the use of bio-based and renewable raw materials has aroused great attention. New type of bio-based aerogels derived from polysaccharide,[29,30] pectin,[31,32] and cellulose[33,34] have

C. Wang, F. Eisenreich, Ž. Tomović
Polymer Performance Materials Group
Department of Chemical Engineering and Chemistry
Eindhoven University of Technology
Eindhoven, MB 5600, The Netherlands
E-mail: z.tomovic@tue.nl
Ž. Tomović
Institute for Complex Molecular Systems (ICMS)
Eindhoven University of Technology
Eindhoven, MB 5600, The Netherlands
The ORCID identification number(s) for the author(s) of this article can be found under https://doi.org/10.1002/adma.202209003.

DOI: 10.1002/adma.202209003

been developed as sustainable equivalents to lower the environmental impact. Moreover, reusing aerogels in a series of consecutive procedures reduces the burden of manufacturing energy. Reusable organic aerogels have been used for oil/water separation purposes[35–37] and heterogenous catalysis.[38–41] However, reapplying these materials eventually follows a linear economy, in which the products are discarded after their end-of-life and their feedstock value is lost. In stark contrast, the development of fully recyclable aerogels would provide the means for a sustainable circular economy. Through selective depolymerization, the monomeric building blocks can be retrieved and subsequently employed in creating fresh aerogel networks, ideally without loss of product quality and resources. Yet, chemical recycling of organic aerogels is exceptionally difficult to achieve due to their highly cross-linked network topology and thus remains experimentally unattained to date. Efficient depolymerization methods to chemically recycle thermoset materials, other than aerogels, have been devised and can serve as a source of inspiration.[42–44] Among them, the design for recycling approach is an attractive strategy which encompasses the introduction of reversible covalent linkages to fabricate novel thermosets and ensures their recyclability under selected conditions.[45,46] Reversible covalent imine bonds, which are defined by their condensation and hydrolysis equilibrium, have extensively been applied to bestow recyclability on polymers[47–51] and also proven to be suitable for the formation of aerogel network.[52,53]

Herein, we disclose the synthesis and characterization of new organic polyimine aerogels (PIAs) consisting of bio-based components that are fully recyclable on demand. A simple, catalyst-free sol–gel process with multifunctional cyclophosphazene-based aldehydes and primary amines followed by supercritical drying was used to successfully prepare a set of PIAs (**Figure 1**). Their delicate nanostructure was verified by low linear shrinkage (<15%), high porosity (>89%), and large surface area (≈170 $m^2 g^{-1}$). Closed-loop recycling of these highly cross-linked polymeric networks was achieved by applying acidic conditions to induce the selective cleavage of imine bonds. The high yielding recovery (of up to 95%) of pure aldehyde and amine monomers allows to prepare fresh aerogels and thus showcases the full potential of our circular materials. This work is the first aerogel study in which recyclability is included as a core feature in the design of high-performance aerogels, in addition to low thermal conductivity, high thermal stability, and great flame retardancy.

2. Result and Discussion

2.1. Design and Fabrication of PIAs

For the construction of highly cross-linked polyimine aerogels, we selected aldehyde decorated cyclophosphazenes (HVP and HBP) in combination with *tris*(2-aminoethyl)amine (TREN) and 2-ethylhexylamine (2-EHA) as suitable monomers (**Figure 2**a). To lower the environmental impact of our materials, the cyclophosphazene rings of HVP and HBP were substituted with bio-based phenolic reagents (i.e., vanillin and 4-hydroxybenzaldehyde), derived from lignin representing one of the most produced renewable biomacromolecules.[54] These cyclophosphazene derivatives not only serve as multifunctional aldehyde precursors for creating dense polyimine networks, but also act as intumescent flame retardant building blocks.[55,56] The tri-functional amine TREN was used as cross-linker, while the incorporation of 2-EHA is expected to improve the hydrophobicity of the PIAs. By elevating the overall hydrophobicity, the porous materials are less susceptible to moisture uptake, which is a crucial parameter to ensure long-term performance of polyimine networks. For our study, we prepared aerogels PIA-A1 and PIA-B1, which are composed of TREN as well as HVP and HBP, respectively. To improve the hydrophobicity, PIA-A2 and PIA-B2 were made by partially replacing TREN with 2-EHA. The optimal composition for the 2-EHA addition was found to be 30 mol% for PIA-A2 and 20 mol% for PIA-B2 (a detailed discussion is disclosed in the Supporting Information).

First, HVP and HBP were employed in polycondensation reactions by mixing them with the amine reagents, respectively, in *N,N*-dimethylacetamide (DMAc) at 80 °C for 2 h (Table S1, Supporting Information). The obtained organogels were further cured overnight at room temperature to ensure full conversion to polyimines (Figure 2b). After exchanging the solvent to acetone, the solvent of organogel was removed by using supercritical CO_2, which is considered as a nontoxic green solvent to conduct supercritical drying.[57] Consequently, ultralight PIAs were successfully prepared with a relatively high content of biorenewable moieties of up to 74 wt% (Table S1, Supporting Information).

The PIAs were analyzed by Fourier transform infrared spectroscopy to confirm the presence of imine bonds. The spectra show characteristic peaks at 1640 cm^{-1} corresponding to C=N stretch absorptions and the absence of signals at 1690 cm^{-1}

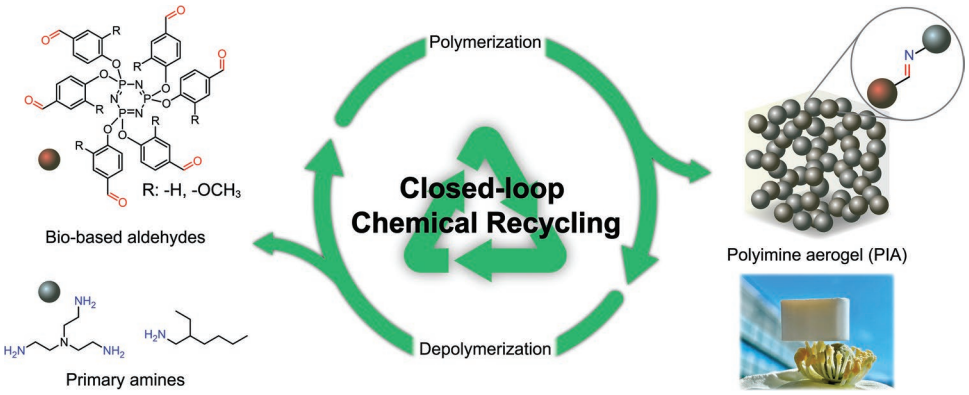

Figure 1. Illustration of the closed-loop recycling scheme of recyclable polyimine aerogels derived from bio-based resources. The photograph shows a PIA sample placed on a flower to demonstrate its low weight.

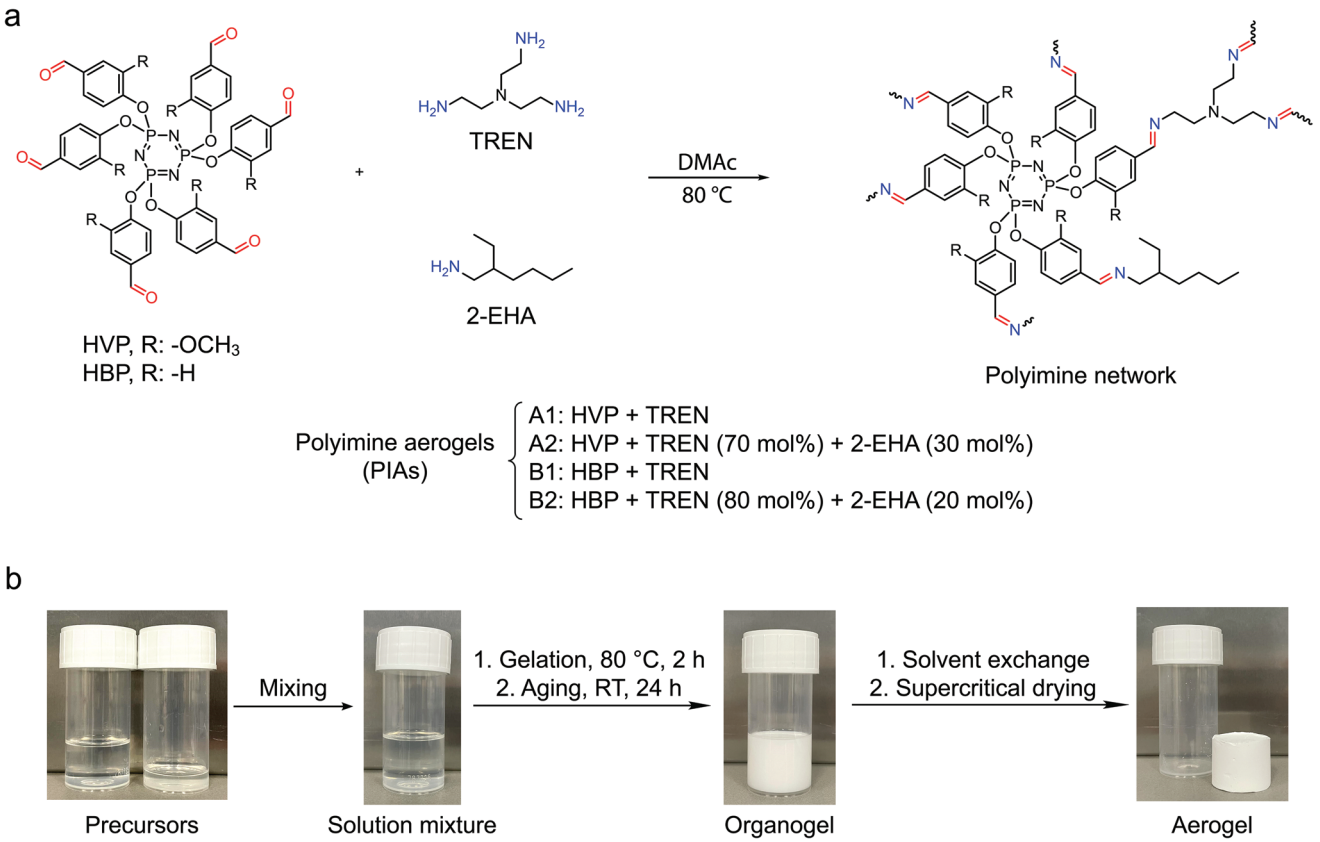

Figure 2. a) Reaction scheme illustrating the condensation reaction of hexavanillin- and hexabenzaldehydecyclophosphazene (HVP and HBP), respectively, with the amines TREN and 2-EHA in different ratios to form cross-linked polyimine networks. b) Schematic representation of the aerogel synthesis protocol. Precursors were dissolved separately in DMAc, mixed at 80 °C for 2 h, and cured overnight at room temperature to obtain stable organogels. The DMAc solvent was exchanged with acetone before supercritical drying with CO_2 was applied to yield PIAs.

which refer to C=O stretch absorptions (Figure S1, Supporting Information), suggesting quantitative formation of imine bonds within the aerogel networks.

2.2. Physical Properties of PIAs

The physical properties of PIAs, including material density, porosity, mechanical properties, and hydrophobicity, are summarized in **Table 1**. The PIAs have successfully been fabricated with low density of ≈0.15 g cm^{-3}. Compared to other organic aerogel in literature, the linear shrinkage after supercritical drying was small (Figure S2, Supporting Information). This behavior may originate from the high cross-link density within the material by using multifunctional precursors. Moreover, the PIAs exhibit significantly high porosities of ≈90%, which is the prerequisite for their air-filling characteristics to create ultralight materials. As for the mechanical properties, PIAs were measured with uniaxial compression to obtain stress-deformation curves (Figure S3a, Supporting Information). The PIAs tolerated high compressive strains without any cracks above 70% deformation ratio (Figure S3b, Supporting Information). Among them, PIA-A2 exhibits the highest compressive strength of 276 kPa and specific modulus of 1.66 m^2 s^{-2} (defined as the ratio of compressive modulus and bulk density). A detailed comparison of PIAs with other organic aerogels in terms of compressive modulus can be found in the Supporting Information (Figure S4, Supporting Information).

Hydrophobicity is one of the most important requirements for the long-term use of the aerogels for various applications. Therefore, harsh water uptake tests were conducted to determine the water affinity of PIAs by immersing them in water for 24 h. PIA-A1 and PIA-B1 showed high water uptake with more than sixfold increase of their original weights, suggesting a strong hydrophilicity (Table 1). In contrast, the incorporation of hydrophobic 2-EHA moieties into the aerogel skeleton greatly improved the inherent water rejecting ability of PIA-A2 and PIA-B2. Their water uptake values are more than 20–30 times lower compared to their fully cross-linked equivalents. The hydrophobicity was further examined by water contact angle measurements. The contact angles for PIA-A2 and PIA-B2 are 127° and 125°, respectively, while the values of PIA-A1 and PIA-B1 are both 0° (Figure S5, Supporting Information). These results align with the water uptake ratio and verify the successful fabrication of hydrophobic PIAs.

The pore structure of PIAs was investigated using nitrogen sorption porosimetry. According to the physisorption isotherms, PIA-A1 has greater adsorbed and desorbed nitrogen values than PIA-B1, indicating a larger mesopore volume (**Figure 3**a). By Brunauer–Emmett–Teller (BET) theory, PIA-A1

Table 1. General material properties of PIAs.

Name	Bulk density ρ_b [mg cm^{-3}][a)]	Linear shrinkage [%][a),b)]	Skeletal density ρ_s [g cm^{-3}a)]	Porosity Π [%][a),c)]	Compressive modulus [kPa][d)]	Specific modulus [m^2 s^{-2}][d)]	Contact angle [°][a)]	Water uptake [%][e)]
PIA-A1	155.8	13.5	1.64	90.52	187 ± 18	1.21	≈0	612
PIA-A2	166.2	14.8	1.55	89.26	276 ± 40	1.66	127	21
PIA-B1	123.7	9.4	1.37	90.97	120 ± 28	0.81	≈0	645
PIA-B2	146.8	15.3	1.36	89.21	203 ± 20	1.64	125	31

[a)]Samples with dimensions of 55 mm diameter and 10 mm thickness were used; [b)]Linear shrinkage was calculated based on the diameter change of the sample; [c)]Porosity was calculated via equation: $\Delta = (1-\frac{\rho_b}{\rho_s}) \times 100\%$; [d)]Compressive modulus was calculated from the stress-deformation curve obtained using sample of 25 mm diameter and 15 mm height, and specific modulus was determined based on the ratio of compressive modulus and ρ_b; [e)]Water uptake ratios were determined by the samples' weight difference before and after submerging in distilled water for 24 h (sample size: 25 mm diameter and 15 mm height).

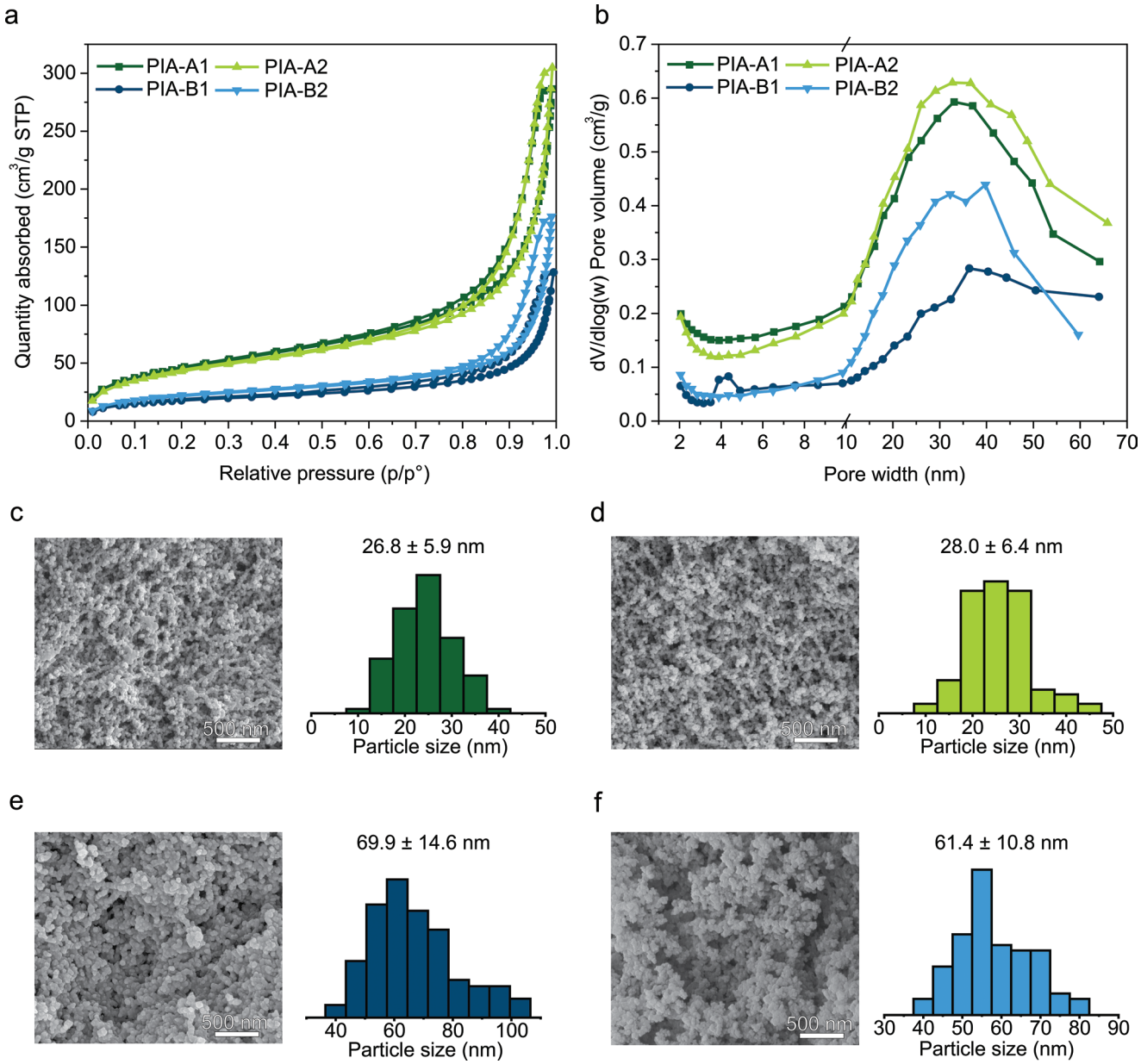

Figure 3. a) N_2 adsorption and desorption isotherms of PIAs at 77 K. b) BJH pore size distribution of PIAs. SEM micrographs and average particle size histograms of c) PIA-A1, d) PIA-A2, e) PIA-B1, and f) PIA-B2.

Table 2. Microstructure and morphology of PIAs.

Name	Specific surface area [m^2 g^{-1}][a)]	Pore volume [cm^3 g^{-1}]	Average pore width [nm][b)]	Average particle size [nm][c)]
PIA-A1	173	0.54	11.6	26.8 ± 5.9
PIA-A2	184	0.59	11.2	28.0 ± 6.4
PIA-B1	90	0.19	8.7	69.9 ± 14.6
PIA-B2	88	0.29	11.2	61.4 ± 10.8

[a)]Calculated based on BET theory; [b)]Calculated using BJH method; [c)]Particles were identified from SEM photographs using Image J software for counting, 100 data points were taken to generate averaged value and standard deviation.

Table 3. Thermal properties of PIAs and reference aerogel.

Name	Thermal conductivity [W m^{-1} K^{-1}] [a)]	$T_{d5\%}$ [°C][b)]	$T_{d30\%}$ [°C][c)]	R_{795} [%][d)]
PIA-A1	0.0182	283	476	42.1
PIA-A2	0.0172	258	411	38.4
PIA-B1	0.0241	311	551	40.7
PIA-B2	0.0220	292	519	40.8
Ref[e)]	0.0179	200	296	21.9

[a)]Thermal conductivity was measured with a heat flow meter (Thermtest Inc., HFM-25); [b–d)]Degradation temperatures for [b)]5% and; [c)]30% weight loss as well as; [d)]char formation yield at 795 °C measured by TGA; [e)]Reference polyurea aerogel was prepared according to literature protocol.[59]

also exhibits a predominantly higher specific surface area. The incorporation of HVP within the structure of PIA-A1 results in more delicate particle-clustered nanostructure compared to HBP-based PIA-B1 (**Table 2**). As per IUPAC classification, the isotherms of PIA-A1 and PIA-B1 display Type IV characteristics, where the hysteresis in the desorption isotherm can be

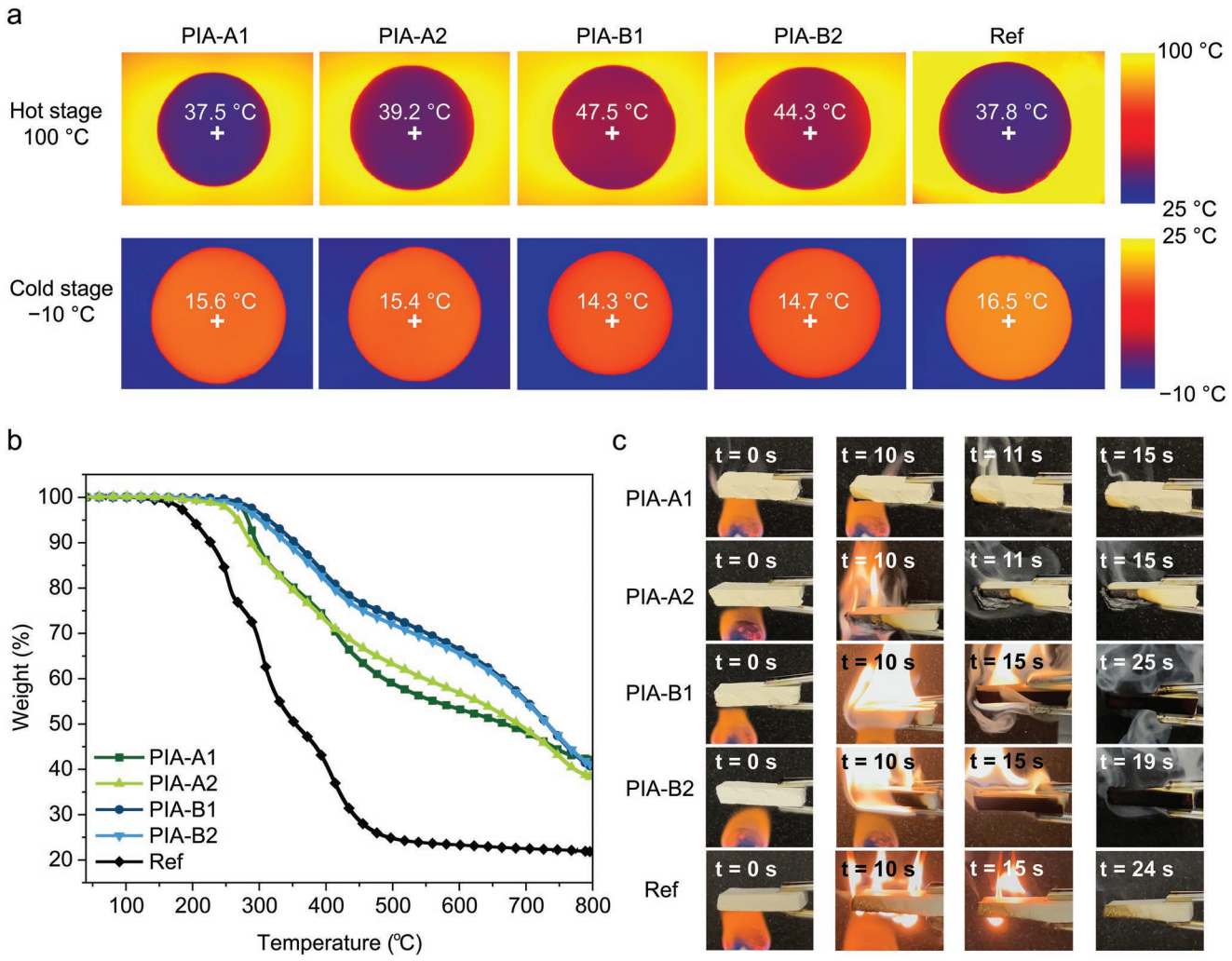

Figure 4. a) Top-view IR images of PIAs and polyurea aerogel (Ref)[59] (10 mm thickness) on hot (100 °C) and cold stage (–10 °C) after 10 min. The middle point temperatures were calibrated by an IR camera. b) TGA curves of PIAs and polyurea aerogel (Ref), ramping from 40 to 795 °C with heating rate of 5 °C min^{-1}. c) Photographs illustrating the burning test of PIAs and polyurea aerogel (Ref). Specimens with 10 mm thickness and 20 mm width were set up horizontally and the bottom of the specimens was exposed to an ethanol burner for 10 s. These tests were recorded and video material can be found in the Supporting Information (Movies S1–S5).

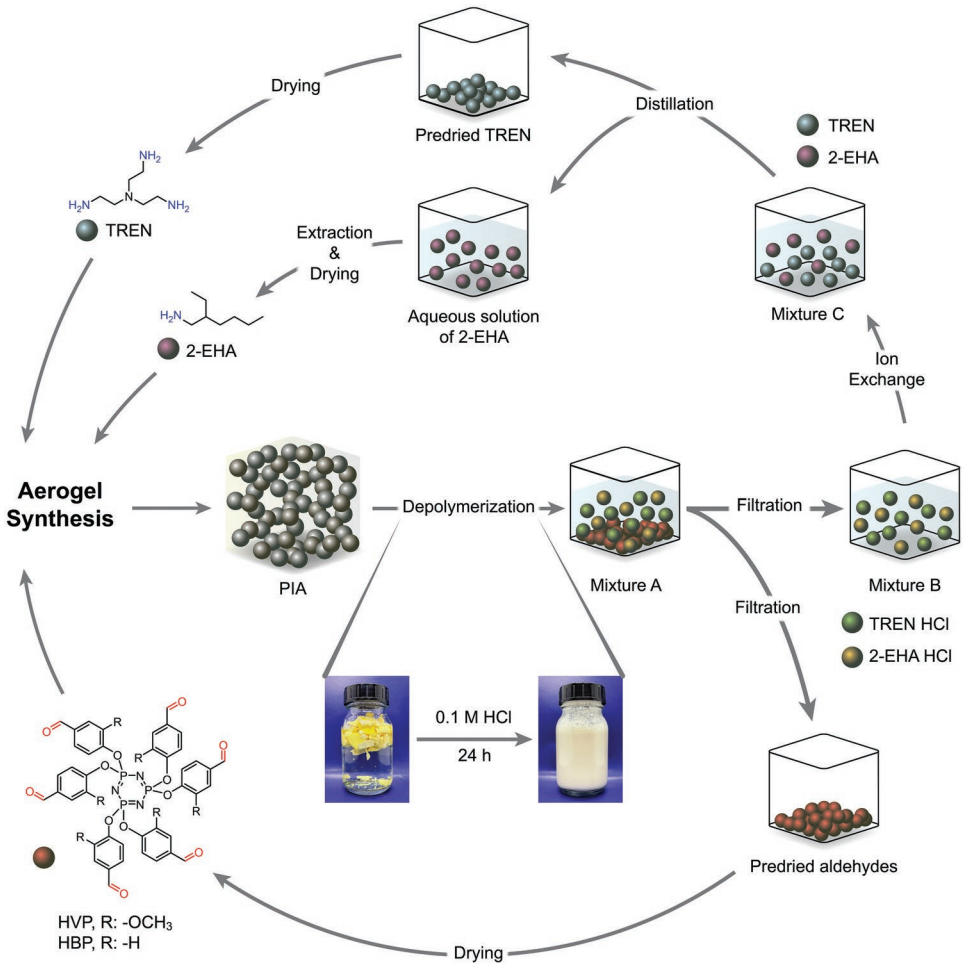

Figure 5. Complete closed-loop recycling scheme for PIA-A2 and PIA-B2. First, PIAs were fabricated from HVP/HBP and amines via aerogel synthesis. Quantitative and selective depolymerization was achieved under acidic condition at room temperature (0.1 M HCl). After filtering mixture A and subsequently drying the aldehyde precursors, pure monomers HVP and HBP were retrieved, respectively. The aqueous mixture B, containing the HCl salts of TREN and 2-EHA, was treated with an ion exchange resin to remove the chloride anions. After distilling water and 2-EHA simultaneously from mixture C, pure TREN was obtained after drying. The aqueous solution of 2-EHA was extracted with ethyl acetate to yield pure monoamine after drying.

seen around the region p/p^0 >0.7, suggesting a great range of different mesopore sizes.[58] By using Barrett–Joyner–Halenda (BJH) analysis, the mesopore size distribution ranges from 20 to 70 nm with relatively high pore volume (Figure 3b). A similar trend was also found between PIA-A2 and PIA-B2 as their pore size and volume are affected by the type of aldehyde precursor.

The morphology of PIAs was studied by scanning electron microscopy (SEM, Figure 3c–f). The SEM images illustrate isotropic nanoscale architectures over a large range and highly porous networks with bead-like morphology. These observations validate that supercritical drying kept the nanostructure intact without damaging the infrastructure by solvent evaporation. The solid particles are composed of spherical or hemispherical contours embedded to a necklace-like skeleton. Measuring the particle sizes among the PIAs showed that PIA-As possess much smaller particle aggregates than PIA-Bs (Table 2). Hence, the complementary pores formed by PIA-As' particles are much more delicate, which is in line with the nitrogen porosimetry data.

2.3. Thermal Properties of PIAs

Owing to the nanoscale topology and the intertwined Knudsen effect, PIAs are expected to show outstanding thermal insulation efficiency.[6,8,9] We measured their thermal conductivity with a heat flow meter according to ASTM C518 standard (**Table 3**). The PIA-A pair exhibits low thermal conductivities with values of ≈0.018 W m^{-1} K^{-1}, while the values for the PIA-B couple of ≈0.024 W m^{-1} K^{-1} are slightly larger. Thus, our PIAs show an insulation performance which is on the same level as the best commercial polyurea aerogels[59,60] and superior to other organic aerogels reported in literature (Figure S6, Supporting Information). Furthermore, we used an IR camera to capture the insulation behavior of PIAs (**Figure 4**a). PIAs and reference polyurea aerogel with 10 mm thickness were put onto a heating/cooling stage and the temperature was set to 100 and −10 °C, respectively. After 10 min, the middle point temperature on the surface of the aerogels was measured. The low thermal conductivities of PIAs restrict the heat transfers through the specimens. As a result, the aerogels' surface temperatures

remain close to room temperature. As the PIA-A couple has a lower thermal conductivity compared to PIA-Bs, their surface temperature is less affected by the heating/cooling stage.

Since the chemical composition of our organic aerogels includes a high content of cyclophosphazene[61,62] and aromatic[63] moieties as well as pronounced cross-linking density,[62] distinct resistance to heat and carbonization ability are expected. We investigated the thermal stability of PIAs using thermogravimetric analysis (TGA, Figure 4b and Table 3). PIAs exhibit high initial degradation temperatures for 5% and 30% weight loss ($T_{d5\%}$ and $T_{d30\%}$) in the range of 258–311 and 411–551 °C, respectively. In addition, PIAs show high char formations with around 40% weight residues at 795 °C (R_{795}). Regarding decomposition temperature and char yield value, PIAs show a significantly elevated thermal stability compared to the reference polyurea aerogel (Ref).[59] Interestingly, the PIA-B pair generally decomposes at higher temperatures than the PIA-A samples. Considering the low activation energy, the methoxy group is prone to be cleaved from the vanillin moiety.[64] As for the hydrophobic aerogels, PIA-A2 and PIA-B2 show slightly lower decomposition temperatures and char residue values compared to the fully cross-linked counterparts. The addition of monoamine lowers the overall cross-link density, which generally has an impact on the thermal resistance of polymeric materials.[62,65,66]

To further investigate the flame retardancy of PIAs and compare with the reference polyurea aerogel, we conducted initial burning tests by exposing specimens to an open flame for 10 s (Figure 4c and Movies S1–S5, Supporting Information).[67–69] After initial ignition, the combustion of PIA-A1 and PIA-A2 stopped almost immediately, while PIA-B1, PIA-B2, and reference material burned slightly longer (9–15 s). The fact that the combustion was extinguished in short time can be attributed to the pronounced flame resistance and compact char formation of PIAs (Figure S7, Supporting Information). The incorporated cyclophosphazenes act as acid and gas sources for intumescent flame retardants,[55,56,61] thereby accelerating char formation and suppressing the combustion. Besides, these results are in line with previous studies in literature, in which vanillin-based materials show better flame retardant behavior than the 4-hydroxybenzaldehyde-based ones.[70,71]

2.4. Closed-Loop Recycling of PIAs

The incorporation of reversible imine bonds into the aerogel network enables efficient depolymerization on demand and thus paves the way for establishing a closed-loop recycling scheme for advanced aerogel materials (**Figure 5**). To illustrate the chemical recycling of polyimine aerogels, we cut samples of PIAs into small pieces and exposed them to an aqueous 0.1 M HCl solution at room temperature for 24 h. Under these acidic conditions, the imine bonds hydrolyze and the polymeric networks break down in a quantitative and selective fashion. As a result, the aldehyde monomers formed precipitates in the aqueous mixture while the HCl salts of the primary amines remained dissolved. Filtration of the mixtures allowed to conveniently isolate the solid HVP and HBP monomers with recovery yields of 83–95% (Table S2, Supporting Information). The acidic filtrate was treated with an ion exchange resin to remove the chloride anions and provide neutral amines. As for PIA-A1 and PIA-B1, pure TREN was obtained after removing the water. In case of PIA-A2 and PIA-B2, monoamine 2-EHA and water were simultaneously separated from TREN through reduced pressure distillation. Pure 2-EHA was collected through extraction with ethyl

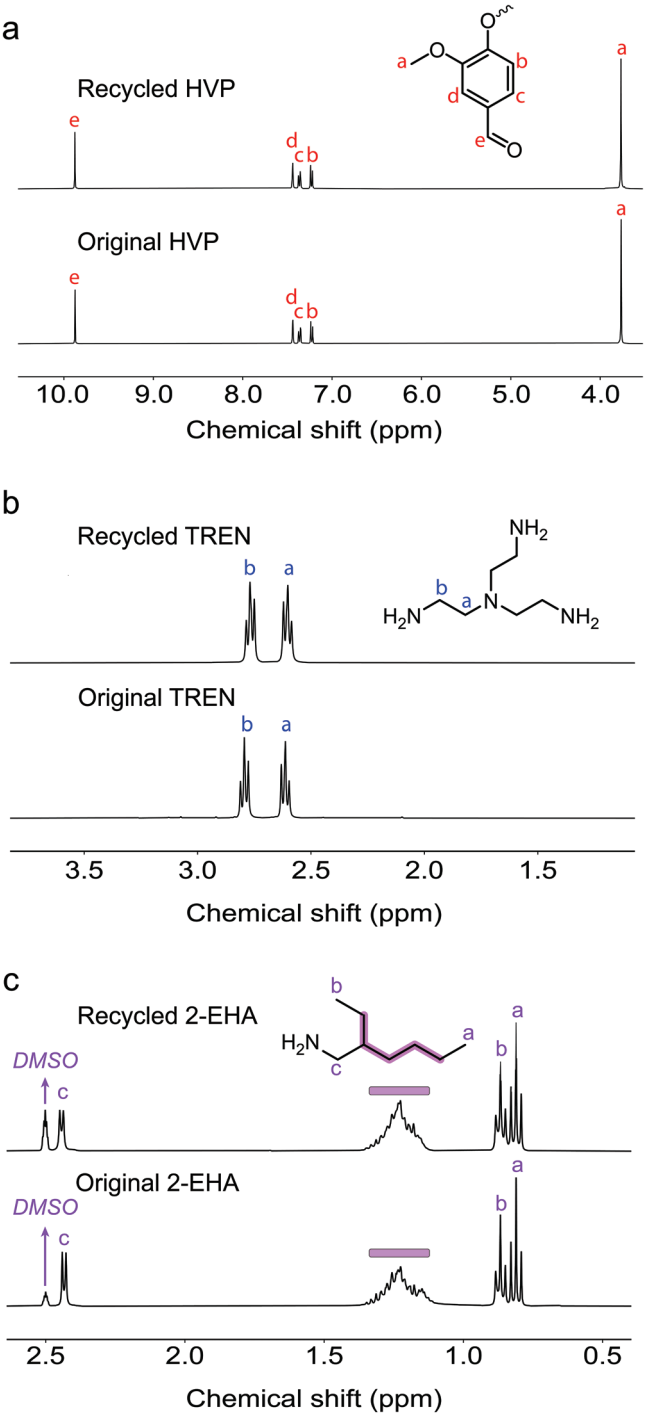

Figure 6. ^{1}H NMR spectra of original and recycled monomers from PIA-A2. a) ^{1}H NMR spectra of original (bottom) and recycled HVP (top) in DMSO-d_6. b) ^{1}H NMR spectra of original (bottom) and recycled TREN (top) in D_2O. c) ^{1}H NMR spectra of original (bottom) and recycled 2-EHA (top) in DMSO-d_6.

acetate and drying. The recovery yields of TREN range from 77% to 91%. Due to the smaller quantities used of 2-EHA and its volatility, the recovery yields of the monoamine are lower with values ranging from 41% to 51%. The purity of all recycled monomers was estimated to be >99% by ^{1}H NMR spectroscopy. Since the isolated and virgin-like monomers are ready to be immediately used again, the preparation of fresh PIAs is enabled (**Figure 6**a–c and Figure S8, Supporting Information).

3. Conclusion

To conclude, we present the first example of closed-loop recyclable organic aerogels derived from bio-based resources. The introduction of reversible imine bonds to the polymeric aerogel network facilitates the on demand depolymerization under mild energy-efficient conditions. Our straight-forward recycling protocol allows to retrieve the original monomers in high purity, thus enabling the preparation of new generations of aerogels in a sustainable fashion. Although the reversibility of imine linkages is well understood and facilitated the preparation of a wide spectrum of recyclable polymers, it has not been applied to create recyclable and advanced aerogel materials to date. Irrespective of the C=N bonds, the PIAs display excellent characteristics, including low linear shrinkage (<15%), high porosity (>89%), large surface area (≈170 m^2 g^{-1}), and elevated hydrophobicity (water contact angle >120°). By incorporating phosphorus- and nitrogen-rich aromatic precursors, PIAs also showcase outstanding thermal stability and great flame retardancy, which is generally considered a weak point of organic aerogels. Their thermal insulation properties are on par with the best commercial polyurea aerogels[59,60] and outperform other literature known organic aerogels.[13,16] This work is expected to spark the development of a circular aerogel economy and drive research on environmentally friendly aerogel materials forward.

4. Experimental Section

The experimental details have been provided in the Supporting Information.

Supporting Information

Supporting Information is available from the Wiley Online Library or from the author.

Acknowledgements

The authors are grateful to Dr. Ingeborg Schreur-Piet (Eindhoven University of Technology, Eindhoven, The Netherlands) for scanning electron microscopy (SEM) measurements and Dr. Xianwen Lou (Eindhoven University of Technology, Eindhoven, The Netherlands) for MALDI-TOF MS characterization. Ž.T. appreciates the support from Gravitation Program Interactive Polymer Materials 024.005.020, The Netherlands Organization for Scientific Research (NWO).

Note: The value for linear shrinkage for the PIA-B1 sample was corrected to 9.4% (instead of 915.3 as when originally published) on February 23, 2023, after initial publication online.

Conflict of Interest

The authors declare no conflict of interest.

Data Availability Statement

The data that support the findings of this study are available from the corresponding author upon reasonable request.

Keywords

aerogels, closed-loop recycling, nanomaterials, polyimine, superinsulation, sustainability, thermal stability

Received: September 29, 2022
Revised: December 5, 2022
Published online: December 23, 2022

[1] T. Li, Y. Zhai, S. He, W. Gan, Z. Wei, M. Heidarinejad, D. Dalgo, R. Mi, X. Zhao, J. Song, J. Dai, C. Chen, A. Aili, A. Vellore, A. Martini, R. Yang, J. Srebric, X. Yin, L. Hu, *Science* **2019**, *364*, 760.
[2] M. Koebel, A. Rigacci, P. Achard, *J. Sol-Gel Sci. Technol.* **2012**, *63*, 315.
[3] N. Hüsing, U. Schubert, *Angew. Chem., Int. Ed.* **1998**, *37*, 22.
[4] M. Aegerter, N. Leventis, M. Koebel, *Aerogels Handbook*, Springer, New York **2011**.
[5] B. P. Jelle, R. Baetens, A. Gustavsen, in *The Sol-Gel Handbook: Synthesis, Characterization, and Applications*, 1st ed. (Eds: D. Levy, M. Zayat), Wiley-VCH, Weinheim, Germany **2015**, pp. 1385–1412.
[6] L. B. Apostolopoulou-Kalkavoura, V. Munier, P. Bergström, *Adv. Mater.* **2021**, *33*, 2001839.
[7] D. Kumar, M. Alam, P. X. W. Zou, J. G. Sanjayan, R. A. Memon, *Renewable Sustainable Energy Rev.* **2020**, *131*, 110038.
[8] K. Malek, M. O. Coppens, *J. Chem. Phys.* **2003**, *119*, 2801.
[9] B. Notario, J. Pinto, E. Solorzano, J. A. De Saja, M. Dumon, M. A. Rodríguez-Pérez, *Polymer* **2015**, *56*, 57.
[10] R. W. Pekala, *J. Mater. Sci.* **1989**, *24*, 3221.
[11] A. Rigacci, J. C. Marechal, M. Repoux, M. Moreno, P. Achard, *J. Non-Cryst. Solids* **2004**, *350*, 372.
[12] C. Chidambareswarapattar, P. M. McCarver, H. Luo, H. Lu, C. Sotiriou-Leventis, N. Leventis, *Chem. Mater.* **2013**, *25*, 3205.
[13] N. Diascorn, S. Calas, H. Sallée, P. Achard, A. Rigacci, *J. Supercrit. Fluids* **2015**, *106*, 76.
[14] N. Leventis, C. Sotiriou-Leventis, N. Chandrasekaran, S. Mulik, Z. J. Larimore, H. Lu, G. Churu, J. T. Mang, *Chem. Mater.* **2010**, *22*, 6692.
[15] N. Leventis, *Polymers* **2022**, *14*, 969.
[16] M. A. B. Meador, E. J. Malow, R. Silva, S. Wright, D. Quade, S. L. Vivod, H. Guo, J. Guo, M. Cakmak, *ACS Appl. Mater. Interfaces* **2012**, *4*, 536.
[17] B. N. Nguyen, M. A. B. Meador, D. Scheiman, L. McCorkle, *ACS Appl. Mater. Interfaces* **2017**, *9*, 27313.
[18] S. L. Vivod, M. A. B. Meador, C. Pugh, M. Wilkosz, K. Calomino, L. McCorkle, *ACS Appl. Mater. Interfaces* **2020**, *12*, 8622.
[19] Y. Deng, Y. Pan, Z. Zhang, Y. Fu, L. Gong, C. Liu, J. Yang, H. Zhang, X. Cheng, *Adv. Funct. Mater.* **2022**, *32*, 2016176.
[20] R. W. Pekala, C. T. Alviso, J. D. LeMay, *J. Non-Cryst. Solids* **1990**, *125*, 67.
[21] M. Moner-Girona, E. Martínez, A. Roig, J. Esteve, E. Molins, *J. Non-Cryst. Solids* **2001**, *285*, 244.
[22] K. Shang, J. C. Yang, Z. J. Cao, W. Liao, Y. Z. Wang, D. A. Schiraldi, *ACS Appl. Mater. Interfaces* **2017**, *9*, 22985.

[23] G. C. Ruben, R. W. Pekala, *J. Non-Cryst. Solids* **1995**, *186*, 219.
[24] P. Lorjai, T. Chaisuwan, S. Wongkasemjit, *J. Sol-Gel Sci. Technol.* **2009**, *52*, 56.
[25] Q. Ma, H. Wang, G. Zhan, X. Liu, Y. Yang, Q. Zhuang, J. Qian, *ACS Appl. Polym. Mater.* **2021**, *3*, 2352.
[26] S. Xiong, Y. Yang, S. Zhang, Y. Xiao, H. Ji, Z. Yang, F. Ding, *ACS Appl. Nano Mater.* **2021**, *4*, 7280.
[27] S. Donthula, C. Mandal, T. Leventis, J. Schisler, A. M. Saeed, C. Sotiriou-Leventis, N. Leventis, *Chem. Mater.* **2017**, *29*, 4461.
[28] D. A. Khanin, Y. N. Kononevich, M. N. Temnikov, V. P. Morgalyuk, V. G. Vasil'ev, A. Y. Popov, V. K. Brel, V. S. Papkov, A. M. Muzafarov, *Polymer* **2020**, *186*, 122011.
[29] K. Ganesan, T. Budtova, L. Ratke, P. Gurikov, V. Baudron, I. Preibisch, P. Niemeyer, I. Smirnova, B. Milow, *Materials* **2018**, *11*, 2144.
[30] C. A. García-González, M. Alnaief, I. Smirnova, *Carbohydr. Polym.* **2011**, *86*, 1425.
[31] C. Rudaz, R. Courson, L. Bonnet, S. Calas-Etienne, H. Sallée, T. Budtova, *Biomacromolecules* **2014**, *15*, 2188.
[32] S. Groult, T. Budtova, *Eur. Polym. J.* **2018**, *108*, 250.
[33] H. Tu, M. Zhu, B. Duan, L. Zhang, *Adv. Mater.* **2021**, *33*, 2000682.
[34] V. Rahmanian, T. Pirzada, S. Wang, S. A. Khan, *Adv. Mater.* **2021**, *33*, 2102892.
[35] H. Bi, Z. Yin, X. Cao, X. Xie, C. Tan, X. Huang, B. Chen, F. Chen, Q. Yang, X. Bu, X. Lu, L. Sun, H. Zhang, *Adv. Mater.* **2013**, *25*, 5916.
[36] Z. Y. Wu, C. Li, H. W. Liang, Y. N. Zhang, X. Wang, J. F. Chen, S. H. Yu, *Sci. Rep.* **2014**, *4*, 4079.
[37] Y. Sun, Y. Li, B. Chen, M. Cui, W. Xu, L. Li, M. Wang, Y. Zhang, K. Chen, Q. Du, Y. Wang, X. Pi, *ChemistrySelect* **2022**, *7*, 202201216.
[38] W. Liu, P. Rodriguez, L. Borchardt, A. Foelske, J. Yuan, A. K. Herrmann, D. Geiger, Z. Zheng, S. Kaskel, N. Gaponik, R. Kötz, T. J. Schmidt, A. Eychmüller, *Angew. Chem., Int. Ed.* **2013**, *52*, 9849.
[39] Z. Luo, Y. Fang, M. Zhou, X. Wang, *Angew. Chem., Int. Ed.* **2019**, *58*, 6033.
[40] B. Cai, A. Eychmüller, *Adv. Mater.* **2019**, *31*, 1804881.
[41] Y. Li, C. K. Peng, H. Hu, S. Y. Chen, J. H. Choi, Y. G. Lin, J. M. Lee, *Nat. Commun.* **2022**, *13*, 1143.
[42] A. R. Rahimi, J. M. Garciá, *Nat. Rev. Chem.* **2017**, *1*, 0046.
[43] G. W. Coates, Y. D. Y. L. Getzler, *Nat. Rev. Mater.* **2020**, *5*, 501.
[44] Y. Jin, Z. Lei, P. Taynton, S. Huang, W. Zhang, *Matter* **2019**, *1*, 1456.
[45] P. R. Christensen, A. M. Scheuermann, K. E. Loeffler, B. A. Helms, *Nat. Chem.* **2019**, *11*, 442.
[46] M. Häußler, M. Eck, D. Rothauer, S. Mecking, *Nature* **2021**, *590*, 423.
[47] P. Taynton, K. Yu, R. K. Shoemaker, Y. Jin, H. J. Qi, W. Zhang, *Adv. Mater.* **2014**, *26*, 3938.
[48] Y. Wang, A. Xu, L. Zhang, Z. chen, R. Qin, Y. Liu, X. Jiang, D. Ye, Z. Liu, *Macromol. Mater. Eng.* **2022**, *307*, 2100893.
[49] K. Saito, F. Eisenreich, T. Türel, Ž. Tomović, *Angew. Chem., Int. Ed.* **2022**, *61*, e202211806.
[50] A. Liguori, M. Hakkarainen, *Macromol. Rapid Commun.* **2022**, *43*, e202100816.
[51] K. Hong, Q. Sun, X. Zhang, L. Fan, T. Wu, J. Du, Y. Zhu, *ACS Sustainable Chem. Eng.* **2022**, *10*, 1036.
[52] J. Zhang, L. Liu, H. Liu, M. Lin, S. Li, G. Ouyang, L. Chen, C. Y. Su, *J. Mater. Chem. A* **2015**, *3*, 10990.
[53] J. Martín-Illán, D. Rodríguez-San-Miguel, O. Castillo, G. Beobide, J. Perez-Carvajal, I. Imaz, D. Maspoch, F. Zamora, *Angew. Chem., Int. Ed.* **2021**, *60*, 13969.
[54] C. Li, X. Zhao, A. Wang, G. W. Huber, T. Zhang, *Chem. Rev.* **2015**, *115*, 11559.
[55] S. Lu, I. Hamerton, *Prog. Polym. Sci.* **2002**, *27*, 1661.
[56] T. Liu, J. Peng, J. Liu, X. Hao, C. Guo, R. Ou, Z. Liu, Q. Wang, *Composites, Part B* **2021**, *224*, 109188.
[57] P. G. Jessop, W. Leitner, in *Chemical Synthesis using Supercritical Fluids*, (Eds: P. G. Jessop, W. Leitner), Wiley-VCH, Weinheim, Germany **1999**, Ch. 1.
[58] J. C. P. Broekhoff, *Mesopore Determination from Nitrogen Sorption Isotherms: Fundamentals, Scope, Limitations*, Elsevier Scientific Publishing Company, New York **1979**.
[59] M. Fricke, D. Weinrich, WO 2015144675 A1, **2015**.
[60] M. Fricke, D. Weinrich, SLENTITE® PU aerogels at aerogel-it, https://www.aerogel-it.de/slentite-and-pu-aerogels (accessed: October **2021**).
[61] Y. W. Chen-Yang, S. J. Cheng, B. D. Tsai, *Ind. Eng. Chem. Res.* **1991**, *30*, 1314.
[62] D. K. Chattopadhyay, D. C. Webster, *Prog. Polym. Sci.* **2009**, *34*, 1068.
[63] E. S. Blake, W. C. Hammann, J. W. Edwards, *J. Chem. Eng. Data* **1961**, *6*, 87.
[64] A. M. Verma, N. Kishore, *New J. Chem.* **2017**, *41*, 8845.
[65] Y. Wang, S. Wang, C. Bian, Y. Zhong, X. Jing, *Polym. Degrad. Stab.* **2015**, *111*, 239.
[66] G. F. Levchik, K. Si, S. V. Levchik, G. Camino, C. A. Wilkie, *Polym. Degrad. Stab.* **1999**, *65*, 395.
[67] J. Meng, Y. Zeng, G. Zhu, J. Zhang, P. Chen, Y. Cheng, Z. Fang, K. Guo, *Polym. Chem.* **2019**, *10*, 2370.
[68] L. Yang, A. Mukhopadhyay, Y. Jiao, Q. Yong, L. Chen, Y. Xing, J. Hamel, H. Zhu, *Nanoscale* **2017**, *9*, 11452.
[69] X. Ren, M. Song, J. Jiang, Z. Yu, Y. Zhang, Y. Zhu, X. Liu, C. Li, H. Oguzlu-Baldelli, F. Jiang, *Adv. Eng. Mater.* **2022**, *24*, 2101534.
[70] L. Zhu, J. Ye, W. Lu, Y. Zhang, Z. Jin, *BioResources* **2020**, *16*, 529.
[71] W. Lu, Z. Jin, *Polym. Degrad. Stab.* **2022**, *195*, 109768.